Applied Physics B (2018) 124:223
https://doi.org/10.1007/s00340-018-7092-9

Applied Physics B
Lasers and Optics

Direct and stand-off fabrication of black silicon with enhanced absorbance in the short-wavelength infrared region using femtosecond laser filament

Yue Su[1] · Xuepeng Zhan[1] · Hongwei Zang[1] · Yao Fu[1] · Aiwu Li[1] · Huailiang Xu[1,2] · See-Leang Chin[3] · Pavel Polynkin[4]

Received: 2 June 2018 / Accepted: 29 October 2018 / Published online: 3 November 2018

Abstract
We report on the experimental demonstration of a technique for rapid fabrication of black silicon with enhanced absorption in the short-wavelength infrared (SWIR) region, directly in the ambient air, and at a standoff distance of about 1 m. Our approach is based on the irradiation of a surface of the crystalline silicon, coated by a 100-nm-thick aluminum film, by femtosecond laser pulses that are propagating in the air in the self-channeling regime known as laser filamentation. By adjusting the processing parameters, we achieve up to 50% absorptivity enhancement in the SWIR spectral range between 1.5 and 2.5 μm wavelength, compared to the case when no aluminum coating is applied prior to the laser processing under the otherwise same conditions. Microscopic and elemental analyses of the processed samples suggest that the absorptivity enhancement is due to both the changes in the morphology of the microstructures formed on the sample surface by the laser irradiation and the modification of the energy-band structure of silicon, as a result of aluminum implantation. Our technique could enable rapid and cost-effective fabrication of silicon-based opto-electronic devices for applications in the infrared spectral range.

Keywords Black silicon · Aluminum coating · Absorptivity enhancement · Infrared · Femtosecond laser filamentation

1 Introduction

Silicon is the most widely used semiconductor, forming the material foundation for microelectronics [1]. Applications of silicon in lasers and optoelectronics, however, are limited by its indirect band-gap structure and by the value of the energy bandgap of about 1.1 eV. The latter limitation precludes the use of pure silicon photodetectors and solar cells with light wavelengths above ~ 1.1 μm, e.g., in the technologically important near-infrared (NIR) and mid-infrared (MIR) spectral domains [2]. Another limitation is associated with the high value of refractive index of crystalline silicon, resulting in the high reflectivity of the silicon–air and silicon–vacuum interfaces, across a wide spectral range. Consequently, even when silicon is used with the light that it intrinsically absorbs, a large fraction of the incident radiation is reflected from the silicon surface and does not penetrate into the material.

Both the abovementioned shortcomings can be remedied through the application of various silicon processing techniques. Extension of silicon absorption into the short-wavelength infrared (SWIR) region can be achieved through hyper-doping silicon by ion implantation, followed by annealing [3]. Dopants introduce impurity bands within the bandgap of silicon, enabling subband cascaded absorption channels [4]. Impurity elements commonly used for hyper-doping silicon are chalcogens [5] and transition metals [6]. High reflectivity of the surface of pure silicon can be essentially eliminated through the introduction of microstructures on the silicon surface, by either reactive ion etching [7–9], or wet chemical etching [10, 11], or electrochemical etching [12]. Microstructures

✉ Huailiang Xu
huailiang@jlu.edu.cn

[1] State Key Laboratory of Integrated Optoelectronics, College of Electronic Science and Engineering, Jilin University, Changchun 130012, China

[2] State Key Laboratory of Precision Spectroscopy, East China Normal University, Shanghai 200062, China

[3] Center for Optics, Photonics and Laser (COPL), Laval University, Quebec City, QC G1V 0A6, Canada

[4] College of Optical Sciences, The University of Arizona, Tucson, AZ 85721, USA

on the silicon surface trap incident light and force it to penetrate into the material over many rescattering events.

Little over a decade ago, it has been demonstrated that femtosecond-laser-assisted hyper-doping of silicon by chalcogens results both in the modification of the band structure, with the associated sub-band-gap photoresponse, and in the microstructuring of the silicon surface that results in very low surface reflectivity [13–15]. Thus, produced material, known as black silicon, is a very promising candidate for the fabrication of photodetectors and solar cells that are operative in a very broad spectral range, including NIR and MIR.

Originally, the fabrication of black silicon involved multi-shot irradiation of the pure crystalline silicon sample, placed into a chemical reactor, with femtosecond laser pulses. The required high intensity of the laser beam on the sample's surface was achieved through tight focusing of the laser beam with an objective lens. This processing geometry has three major drawbacks: (1) limited processing speed, due to the small size of the tight focus for the laser beam on the moving sample; (2) the requirement to maintain precise working distance between the focusing objective and the sample; and (3) the inconvenience associated with conducting the processing inside a chemical reactor.

Recently, we have demonstrated that black silicon can be produced directly in the air, at high speed, and at a standoff distance with extremely loose tolerance for the placement of the sample relative to the laser source [16]. The demonstrated technique has the potential to alleviate all three shortcomings (1)–(3) of the original experimental geometry for the fabrication of black silicon mentioned above. It relies on the application of very loosely focused, millijoule-level, femtosecond laser pulses propagating in the air in the self-channeling regime known as laser filamentation [17].

The formation of the femtosecond laser filament relies on the self-focusing of the laser beam, which requires the peak power of the laser pulse to exceed the self-focusing threshold. The value of this threshold power, in the air, is in the range from 3 to 10 GW, depending on the duration of the laser pulse—longer pulses generally have lower values of the threshold. As the beam propagates towards the sample, the transverse collapse of the beam profile due to self-focusing is stopped and balanced, in a dynamic sense, by nonlinear losses to ionization of air molecules and by defocusing of the laser beam by the generated electron plasma. As a result, the laser beam creates a nonlinear waveguide for itself and propagates sub-diffractively over many Rayleigh ranges corresponding to the size of the intense filament core, which is on the order of 100 μm. The sample can be placed anywhere within the range of this nonlinear waveguide, which can be as long as several meters, and where the peak laser intensity is clamped to the relatively constant value on the order of 100 TW/cm^2 [18].

The challenging aspect of material processing with femtosecond laser filaments is that the exact value of the clamped intensity depends on the focal length of the optic used to weakly focus the beam. The use of an external weak focusing is inevitable if we want to confine the interaction zone to the reasonable range on the order of 1 m. As the *f*-number of the focusing optic changes from ~ 100 to ~ 500, the value of the clamped intensity decreases from about 200 TW/cm^2 to about 55 TW/cm^2 [19]. Clamped intensity inside the filament core is determined by the strength of the focusing optic and is largely independent of the energy of the laser pulse. Intensity clamping in the self-channeled laser filament makes the processing insensitive to the exact position of the sample relative to the laser source, but the intensity may be clamped not at the level optimal for the processing.

To address the above challenge, we note that only the ~ 100 μm—wide filament core has the clamped high intensity. The surrounding part of the beam, commonly referred to as ``the photon bath'' or ``the filament reservoir'', propagates essentially linearly and has lower intensity, primarily determined by the linear beam focusing [20]. As we show, by correctly partitioning the processed sample's surface between the filament core and the reservoir, the fabrication process can be optimized and samples with high absorption well below the bandgap of pure silicon can be fabricated. Such a partitioning can be realized by varying the distance between the individual lines produced, on the moving sample, by the laser beam comprising the filament core with high clamped intensity, and the surrounding energy reservoir, with much lower intensity.

In the present study, we experimentally demonstrate that the absorptive properties of black silicon produced in the ambient air by filament processing, as demonstrated in [16], can be further significantly improved through the introduction of an additional straightforward processing step: coating the silicon sample with a 100 nm-thick layer of aluminum. As we show, under certain processing conditions, the laser beam completely removes the aluminum coating through multi-shot ablation. However, the introduction of this sacrificial aluminum layer results in an up to 50% enhancement of the absorptivity of the processed sample in the wavelength range from 1.5 to 2.5 μm when the partitioning of the sample between the filament core and the reservoir is optimized. As our microscopic and elemental analyses show, the enhanced absorptivity is due to both the modifications of the morphology of microstructures formed on the sample's surface by multi-shot laser irradiation, and the laser-assisted implantation of aluminum into the sample. Our findings could potentially enable rapid, standoff fabrication of silicon optoelectronic devices for the use in the SWIR spectral range.

2 Experimental setup

Our experimental setup is shown in Fig. 1. A Ti:sapphire laser system (Spectra-Physics, Spitfire ACE) generates 35 fs—long laser pulses, at 800 nm center wavelength, at the pulse repetition rate of 500 Hz. The laser beam is linearly polarized. The energy of the laser pulses is controlled by the combination of a half-wave plate and a polarizer. The laser beam is focused in the air by a 25.4 mm—diameter, fused-silica lens with the focal length of 100 cm. The resulting laser filament is formed near the focal plane of the lens. The filament has a length of about 3 cm and an estimated diameter of the filament core of about 100 µm. In all fabrication experiments reported here, the laser pulse energy is fixed at 1.6 mJ. Under these conditions, the laser pulse forms a single filament, and thus, the effects associated with the interactions between multiple filaments [21–23] are avoided. The estimated clamped intensity inside the core of the laser filament is between 150 and 200 TW/cm^2 [19], while the intensity in the surrounding reservoir portion of the beam is smaller by a factor between 3 and 4. The corresponding beam fluence is above the single-shot ablation threshold for aluminum, for both the filament core and the reservoir portions of the beam [24].

Black silicon with enhanced absorption in the SWIR region is fabricated from 20 mm × 20 mm, 500-µm-thick, *N*-type silicon (111) wafers, polished on both sides. The wafer is first cleaned, successively, with acetone, ethanol, and deionized water. It is then coated with a 100 nm-thick Al film by a vacuum thermal evaporation technique. For laser processing, the sample is mounted on a three-dimensional moving platform, with the minimum step along both directions within the sample's plane of 2.5 µm and the maximum translation speed of 125 mm/s. The sample is placed within the 3 cm-long laser filament, so that the laser beam strikes the surface of the sample at normal incidence. Black silicon is then produced by moving the sample in the beam, line-by-line. Under optimum processing conditions, that we discuss below, the aluminum surface is completely ablated away from the surface of the sample, both in the filament and in the reservoir portions of the beam. The remnants of the aluminum coating are then cleaned off by placing the sample into a hydrochloric acid solution. As the last processing steps, the sample is cleaned with ethanol and deionized water and dried.

The optical properties of the processed silicon surfaces are measured using a spectrophotometer (UV-3600, Shimadzu Company) equipped with an integrating sphere (LISR-UV), so that both the reflectance (R) and transmittance (T) in the spectral range from 240 nm to 2.5 µm are determined. The absorptance (A) is calculated from the measured data according to the relation $A = 1-R-T$. Note that our spectrometer setup collects all the light scattered by the microstructured surface, both in reflection and in transmission. The absorptance obtained that way equals the absolute fraction of the incident light absorbed within the sample [13, 25]. It should be pointed out that the microstructures processed on the surface of the sample make it impossible to deduce the value of the complex refractive index from the measured reflectance and transmittance spectra.

Following optical characterization, the samples are subjected to microscopic and chemical analyses. The morphology of the microstructures on the silicon surface is analyzed with the help of a field emission scanning electron microscope (SEM model JSM-7500F by JEOL). The type of the solid phases on the surface of the processed samples is analyzed by a Raman spectrometer (model LabRAM HR Evolution by Horriba Scientific), with a 532 nm laser as the excitation light source. The elemental composition analysis is performed using an energy-dispersive spectrometer (EDS model EDAX by AMETEK).

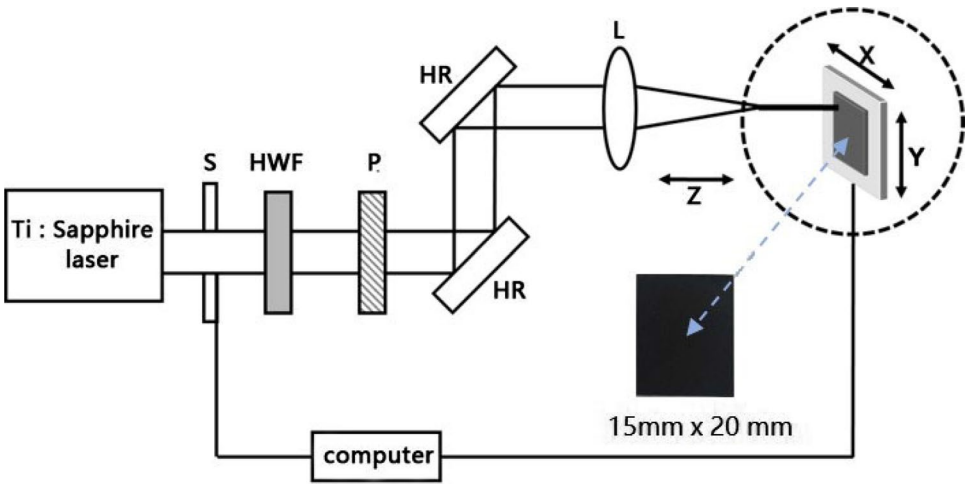

Fig. 1 Schematic diagram of the experimental setup for femtosecond filament processing. *S* shutter, *HWF* half-wave plate, *P* polarizer, *L* fused-silica lens with $f = 100$ cm, *HR* high-reflection mirrors for 800 nm. Inset: photograph of the produced black silicon surface with an area of 15 mm × 20 mm taken by a digital camera

3 Results and discussion

In our experiments, the processing parameters, such as the translation speed of the sample within the laser beam and the distance between the individual processed lines, have been varied to maximize the absorptivity of the processed samples over a wide spectral range. At a fixed repetition rate of the laser pulses, the translation speed determines the number of laser pulses hitting the same spot on the sample's surface, while the distance between the individual lines defines the partitioning of the processed surface between the filament and the reservoir portions of the laser beam.

The absorption spectra for three different intervals between the adjacent processed lines are shown in Fig. 2a–c, for the cases with and without the aluminum coating applied prior to the laser irradiation. The absorption spectra are computed from the measured reflection (Fig. 2a'–c') and transmission (Fig. 2a"–c") spectra using the relation $A = 1 - R - T$. The processing parameters are specified in the figure caption. It is evident from the absorption spectra that (1) there appears to be an optimum with respect to the spacing between the individual processing lines, for both cases with and without aluminum coating and (2) aluminum coating significantly improves the performance of black silicon in the SWIR spectral range.

In Fig. 2b, which shows data for the case of nearly optimum processing with respect to the sample translation speed and the separation between the individual processed lines, the absorption efficiency of the Al-coated sample reaches 90–96% in the spectral range from 240 nm to 1.0 µm, 65–74% in the range 1.2–1.8 µm, and 60–65% in the range 2.0–2.4 µm. As the line separation is increased above ~ 400 µm, the absorptivity declines, as shown in Fig. 2c. This is because in that case, there are completely unprocessed areas left on the sample in between the well-separated individual processed lines.

For all three cases shown in Fig. 2a–c, which correspond to different partitioning of the processed sample between the filament and the reservoir parts of the laser beam, the application of aluminum coating prior to the laser irradiation improves the absorptivity, most notably in the SWIR spectral range. Interestingly, in the SWIR above ~ 1.7 µm

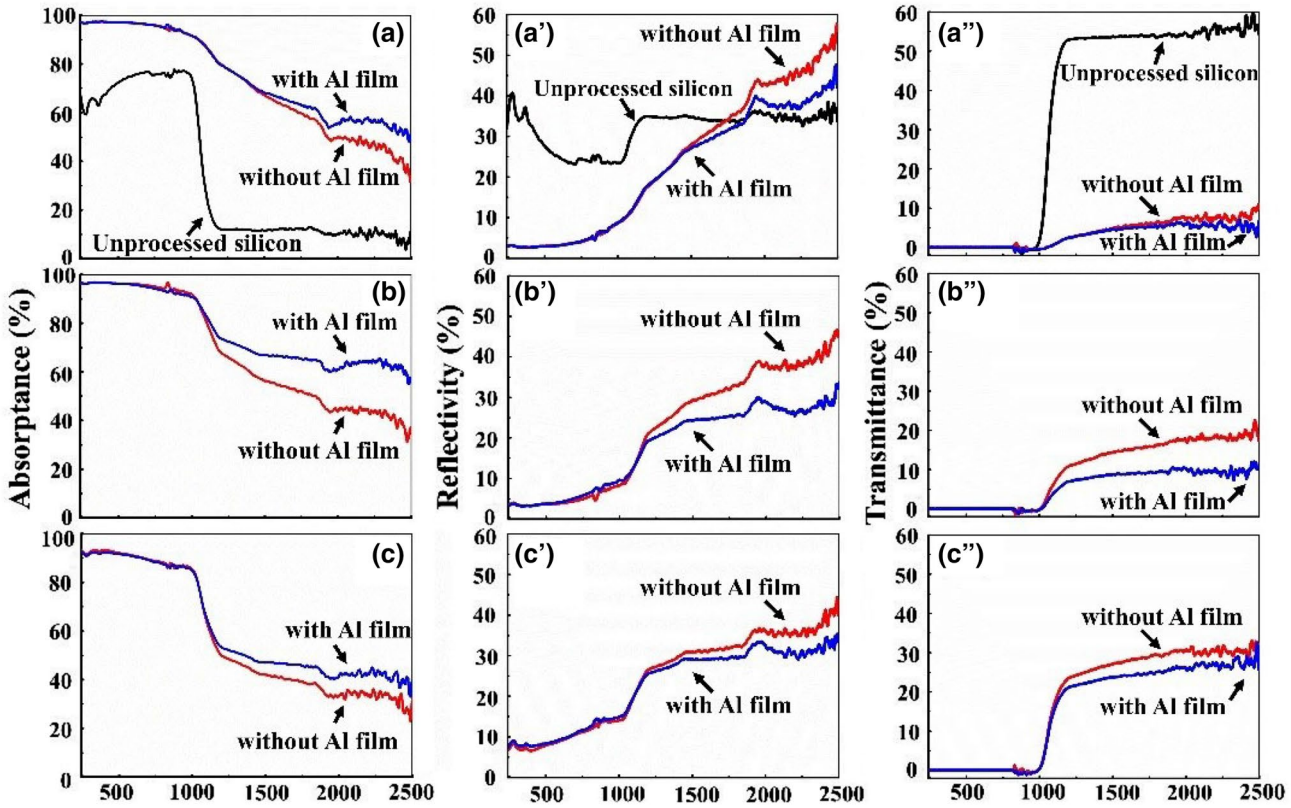

Fig. 2 **a, b, c** Absorption spectra of the fabricated black silicon computed from (**a**', **b**', **c**') reflection and (**a**", **b**", **c**") transmission spectra, under different processing conditions, and for the cases with and without the aluminum coating applied prior to the laser irradiation. Scanning speed is 2.5 mm/s in all cases, corresponding to about 20 laser shots consecutively hitting the same spot on the sample. The distances between individual processed lines are 100 µm (**a, a**','**a**"), 300 µm (**b, b**', **b**"), and 500 µm (**c, c**', **c**"). The data for bare (unprocessed) silicon are also shown, for comparison

wavelength, the laser processing, both with and without Al coating, increases the reflectivity of the samples. At the same time, the measured transmissivity of the samples is reduced significantly, relative to the transmissivity of unprocessed silicon, so that the overall absorption is increased. For the case of Fig. 2b, which shows the data for nearly optimal processing conditions, the maximum improvement of absorption, relative to the case of laser-processed sample without Al coating, is by as much as 50%. The maximum improvement occurs in the wavelength range between 2.0 and 2.5 μm.

To understand the physical mechanisms behind the absorptivity improvement by aluminum coating, we conduct microscopic and elemental analyses of the samples processed under various conditions. SEM images under moderate magnification, shown in Fig. 3, do not reveal any significant differences in the morphology of the microstructures formed on the samples produced with and without the application of aluminum coating. In the case of large separation between the processing lines, parts of the sample between the lines are left entirely unprocessed, as evident from the images shown in Fig. 3c, f. These untreated areas contribute to large reflection from the sample's surface in the UV–visible–NIR range (see Fig. 2a'–c'), corresponding to decreased absorption, as shown in Fig. 2c.

The difference in the surface morphology between the samples processed with and without aluminum coating applied becomes evident in the SEM images at higher magnification, as shown in Fig. 4. Here, panels (a), (a'), (a") are for the case shown in Fig. 3b—optimum laser processing conditions, with aluminum coating, and panels (b), (b'), (b") are for the case shown in Fig. 3e—optimum laser processing conditions, without aluminum coating. In both cases, the morphologies of the microstructures produced by the filament portion of the beam are very similar: The structures are of the mountain-valley type, with the average size of the structures of about 10 μm. The major difference is evident in the areas processed with the reservoir part of the laser beam: in the case with aluminum coating 4(a"), there are relatively large microstructures, with the average size of ~2 to 3 μm, covered by much smaller microstructures, with the average size of ~0.5 to 0.8 μm. Only the smaller microstructures are present in the sample without aluminum coating shown in 4(b"). The relatively larger microstructures shown in

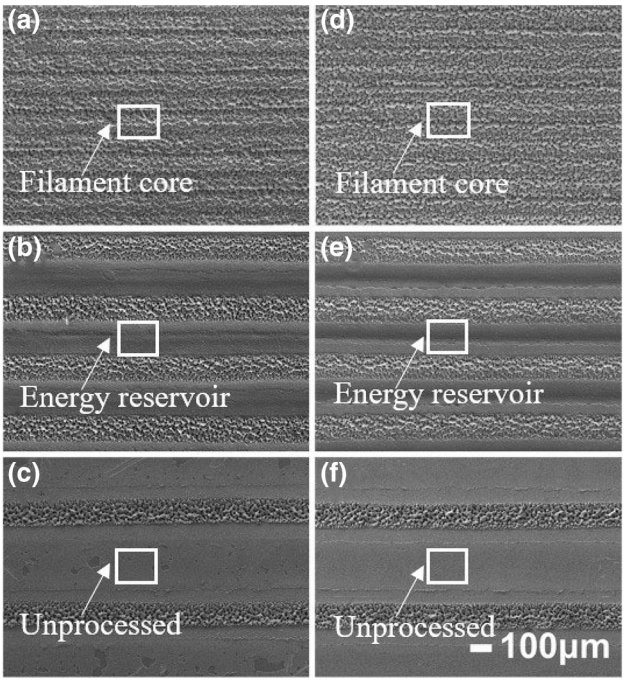

Fig. 3 SEM images of the silicon surfaces, processed with **a**–**c** and without **d**–**f** Al coating, under moderate magnification. The vertical spacing between the adjacent processed lines is 100 μm **a, d**, 300 μm **b, e**, and 500 μm **c, f**, corresponding to the same three cases as those shown in Fig. 2. The areas on the samples that are processed with the filament and the reservoir parts of the laser beam, as well as the unprocessed area on the sample with large separation between the individual processing lines, are marked with rectangles on the individual images

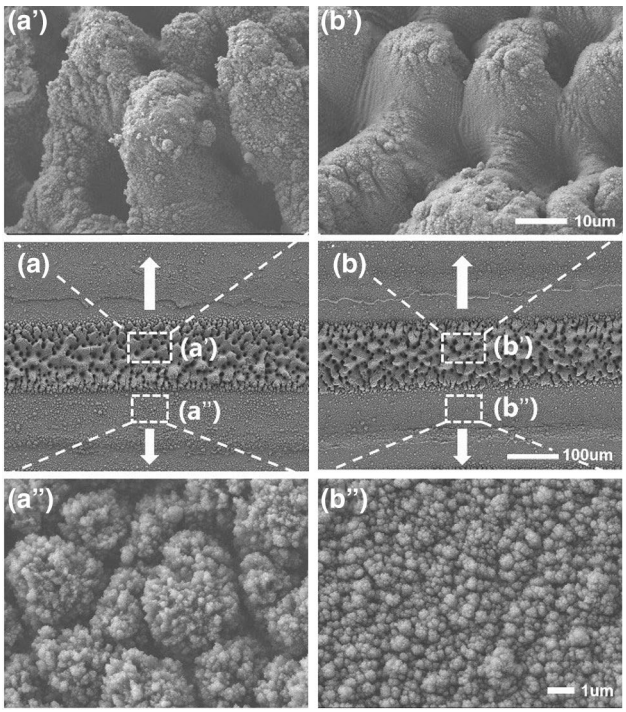

Fig. 4 **a** Top view of the processed sample with aluminum coating. **a**' and **a**": zoomed-in views at 30° view angle, for the areas indicated with rectangles in Fig. 4a. The processing conditions are the same as those used in Fig. 3**b. b, b**', **b**" Same for the processed sample without aluminum coating applied prior to the laser irradiation. The processing conditions are the same as those used in Fig. 3e. The morphology of the microstructures formed on the sample's surface and processed in the reservoir part of the laser beam is strongly affected by the Al coating

Fig. 4a'' may be due to a combined effect of multi-pulse irradiation and Al coating. In Fig. 5, we show the SEM images of the samples processed with the reservoir zone of the beam for the cases with (a–c) and without (d–f) Al coating, at different scanning speeds of 2.5 mm/s (a, d), 5 mm/s (b, e) and 10 mm/s (c, f). It can be clearly seen from Fig. 5a–c that as the scanning speed increases from 2.5 to 10 mm/s, corresponding to 20 laser shots and 5 laser shots hitting the same position on the sample, respectively, the multi-layer microstructures gradually disappear, confirming the multi-pulse effect. In addition, no multi-layer microstructures are formed on the sample without Al coating, as evident from Fig. 5d–f, confirming that the Al film plays an essential role in the formation of the hierarchical microstructures.

Based on the reflectivity data shown in Fig. 2a', b', the observed difference in the morphology of the surface microstructures is sufficient to cause significant reflectivity inhibition in the case of the samples with Al coating. The microstructures formed on the Al-coated sample in the reservoir portion of the laser beam have better light-trapping ability than those made from the samples without Al coating, which may be ascribed to the hierarchy of the multi-layer microstructures in the former case that causes a larger fraction of the light to be scattered into the substrate [25]. Although the same effect as the processing by the reservoir part of the filament can be achieved simply by reducing the energy of the laser. However, in that case, the advantage of long-range propagation in the self-guiding filamentation regime will be lost.

To elucidate the absorption enhancement due to the application of Al coating, we conduct chemical and spectroscopic analyses of the processed samples. The examination of Raman spectra of the samples, shown in Fig. 6, indicates that a phase transformation of silicon occured near the sample surface for both cases of processing with and without Al film. The processing conditions correspond

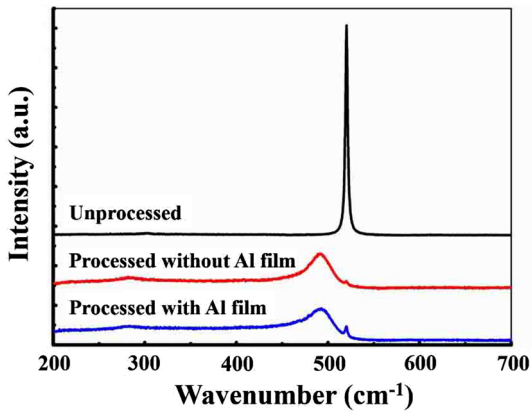

Fig. 6 Raman spectra of the unprocessed silicon, and for the silicon processed with and without aluminum coating

to those used in Figs. 2b and 3b, e. The pronounced spectral peak at 520 cm^{-1} is assigned to the Si-I diamond structure of the crystalline silicon, and the broader peaks at 485–495 cm^{-1} and at 280–300 cm^{-1} are assigned to the amorphous α-Si silicon structure. It is evident from the Raman spectra that the Si-I peak of the crystalline silicon in the processed samples, both with and without aluminum coating, is strongly suppressed. The spectrum is dominated by the peaks assigned to the α-Si, amorphous silicon, suggesting that a partial phase transformation took place near the sample's surface, as a result of the interaction with femtosecond laser pulses. However, although the structure defects in α-Si related to the Urbach states can affect the infrared absorption of black silicon [26], the Raman spectra of black silicon fabricated from the samples with and without aluminum coating are essentially identical, suggesting that the difference between the optical absorption spectra of coated and uncoated samples is not due to the laser-enabled amorphization.

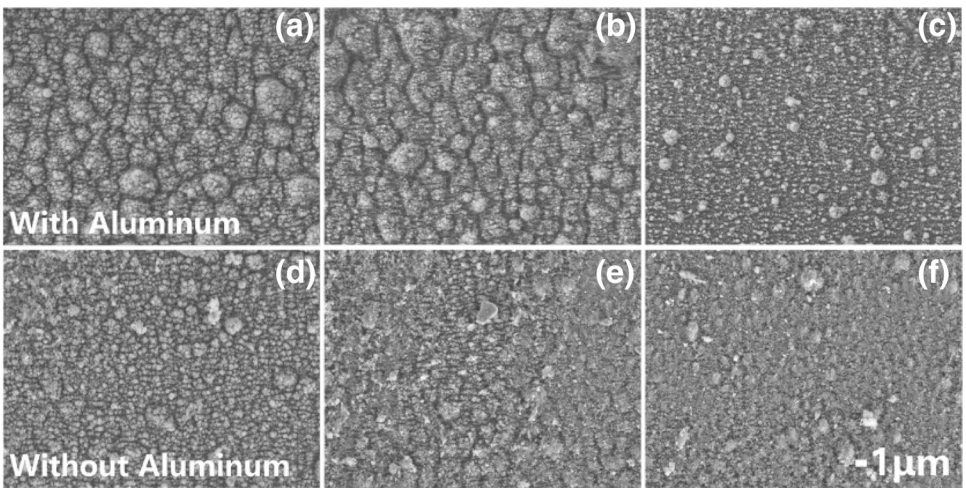

Fig. 5 SEM images of the areas on the sample processed by the energy-reservoir part of the beam, for the cases with **a–c** and without **d–f** Al coating, and at different scanning speeds of 2.5 mm/s (**a, d**), 5 mm/s (**b, e**), and 10 mm/s (**c, f**)

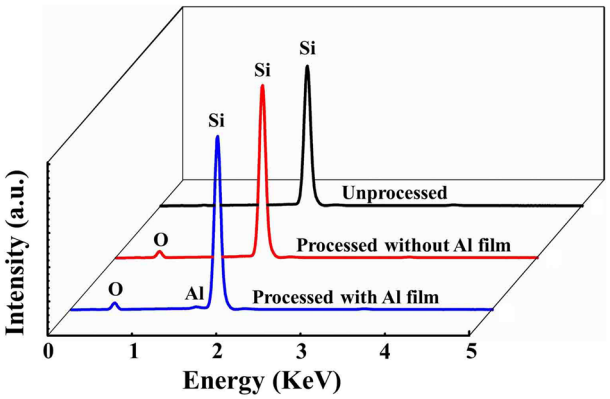

Fig. 7 EDS spectra for the unprocessed silicon, as well as for the processed silicon surfaces with and without Al coating

We further study the chemical composition of the samples by energy-dispersive spectroscopy (EDS). The EDS spectra, shown in Fig. 7, show about 3% content of oxygen in the processed samples, which is indicative of the formation of SiO_x compounds, as a result of laser irradiation in the natural air atmosphere [15, 16]. In the case of the laser-processed sample with aluminum coating, the EDS spectrum shows a small peak at 1.486 eV, which is assigned to aluminum. All aluminum left on the surface of the sample was completely removed by the hydrochloric acid solution. Thus, the observation of aluminum content in the EDS spectrum indicates that the filament processing results in aluminum implantation into the sample, which may result in the modification of the energy-band structure of silicon. Aluminum implantation is the likely cause for the absorption enhancement relative to the case of laser processing without Al coating applied. A similar effect of absorption enhancement in chemically etched, Al-coated silicon films has been recently reported in [27].

4 Summary

In summary, we have investigated a technique for the fabrication of black silicon by the irradiation of the silicon sample by femtosecond laser pulses propagating in the air in the self-channeling (filamentation) regime. We found that when the surface of the silicon sample is coated with an Al film prior to the laser irradiation, the absorptivity in the SWIR spectral range is significantly enhanced. The demonstrated absorption values, under the close-to-optimum processing conditions, are 90–96% in the spectral range 240 nm–1.0 μm, 65–74% in the spectral range 1.2–1.8 μm, and 60–65% in the spectral range 2.0–2.4 μm. By analyzing the processed samples with SEM, we show that the addition of Al coating affects the morphology of the surface microstructures, resulting in the improved light-trapping ability of the black surface. Analyses with the aid of Raman spectroscopy and EDS indicate that the observed absorptivity improvement in the samples prepared with Al coating is likely to be due to the laser-assisted aluminum implantation, which may cause changes in the energy-band structure of silicon through the introduction of defect and impurity bands.

Acknowledgements This work is partially supported by the National Natural Science Foundation of China (61625501, 61427816), the National Basic Research Program of China (2014CB921302), and the Open Fund of the State Key Laboratory of High Field Laser Physics (SIOM). SLC acknowledges the support of COPL, Laval University, Quebec City, Canada. PP acknowledges the support from the United States Air Force Office of Scientific Research (AFOSR, MURI program #FA9550-16-1-0013).

References

1. B. Razavi, *Fundamentals of microelectronics* (Wiley, Hoboken, 2008)
2. R. Nat, Photonics, focus issue on mid-infrared photonics, 6, 407–498 (2012)
3. W. Yang, J. Mathews, J.S. Williams: Mat. Sci. Semicond. Proc. 62, 103–114 (2017)
4. A. Luque, Marti, Phys. Rev. Lett. **78**, 5014 (1997)
5. P. Bob, A. Kohno, S. Charnvanichborikarn, J.M. Warrender, I. Umezu, M. Tabbal, J.S. Williams, M.J. Aziz, J. Appl. Phys. **107**, 123506 (2010)
6. M.J. Recht, S. Smith, J.T. Charnvanichborikarn, M.T. Sullivan, J. Winkler, J.M. Mathews, T. Warrender, J.S. Buonassisi, S. Williams, M.J. Gradevak, Aziz, J. Appl. Phys. **114**, 124903 (2013)
7. Y.F. Huang, S. Chattopadhyay, Y.J. Jen, C.Y. Peng, T.A. Liu, Y.K. Hsu, C.L. Pan, H.C. Lo, C.H. Hsu, Y.H. Chang, C.S. Lee, K.H. Chen, L.C. Chen, Nat. Nanotechnol. **2**, 770–774 (2007)
8. S.H. Zaidi et al., Characterization of random reactive ion etched-textured silicon solar cells. IEEE Trans. Electron. Dev. **48**, 1200 (2001)
9. C. Lee, S.Y. Bae, S. Mobasser, H. Manohara, Nano Lett. **5**, 2438 (2005)
10. S. Koynov, M.S. Brandt, M. Stutzmann, Appl. Phys. Lett. **88**, 203107 (2006)
11. H.M. Branz, V.E. Yost, S. Ward, K.M. Jones, B. To, P. Stradins, Appl. Phys. Lett. **94**, 231121 (2009)
12. Z.P. Wang, G.Y. Feng, S.T. Wang, S.Y. Dai, S.H. Zhou: Optik **128**, 178 (2017)
13. C. Wu, C.H. Crouch, L. Zhao, J.E. Carey, R. Younkin, J.A. Levinson, E. Mazur, R.M. Farrell, P. Gothoskar, A. Karger, Appl. Phys. Lett. **78**, 1850 (2001)
14. J.E. Carey, C.H. Crouch, M. Shen, E. Mazur, Opt. Lett. **30**, 1773 (2005)
15. Y. Vorobyev, C. Guo, Appl. Surf. Sci. **257**, 7291 (2011)
16. X. Zhan, H. Xu, C. Li, H. Zang, C. Liu, J. Zhao, H. Sun, Opt. Lett. **42**, 510 (2017)
17. A. Couairon, A. Mysyrowicz, Phys. Rep. **441**, 47 (2007)
18. V.P. Kandidov, V.Yu. Fedorov, O.V. Tverskoy, O.G. Kosareva, S. L. Chin: Quant. Electr. **41**, 382 (2011)
19. X.L. Liu, W.B. Cheng, M. Petrarca, P. Polynkin, Opt. Lett. **41**, 4751 (2016)
20. W. Liu, F. Theberge, E. Arevalo, J.-F. Gravel, A. Becker, S.L. Chin, Opt. Lett. **30**, 2602 (2005)

21. L.P. Shi, W.X. Li, Y.D. Wang, X. Lu, L. Ding, H.P. Zeng, Phys. Rev. Lett. **107**, 095004 (2011)
22. S. Yuan, T.J. Wang, H.F. Pan, L.J. Zheng, S.L. Chin, H.P. Zeng, Opt. Express **23**, 5582 (2015)
23. S.L. Chin, H.L. Xu, J. Phys. B: At. Mol. Opt. Phys. **49**, 222003 (2016)
24. B. Le Drogoff, F. Vidal, Y.V. Kaenel, M. Chaker, T.W. Johnston, S. Laville, M. Sabsabi, J. Margot, J. Appl. Phys. **89**, 8247 (2001)
25. Y. Nishijima, R. Komatsu, S. Ota, G. Seniutinas, A. Balčytis, S. Juodkazis, APL Photonics **1**, 076104 (2016)
26. C. Li, J. Zhao, Q. Chen, J. Feng, W. Zheng, H. Sun, IEEE Photonics Technol. Lett. **27**, 1481 (2015)
27. Z. Liu, H. Liu, X. Wang, H. Yang, J. Gao: Sci. Rep. **7**, 42750 (2017)